Medical Physics
The International Journal of Medical Physics Research and Practice

Performance of antiscatter grids in diagnostic radiology: Experimental measurements and Monte Carlo simulation studies

HeangPing Chan, Yoshiharu Higashida, and Kunio Doi

Citation: Medical Physics **12**, 449 (1985); doi: 10.1118/1.595670
View online: http://dx.doi.org/10.1118/1.595670
View Table of Contents: http://scitation.aip.org/content/aapm/journal/medphys/12/4?ver=pdfcov
Published by the American Association of Physicists in Medicine

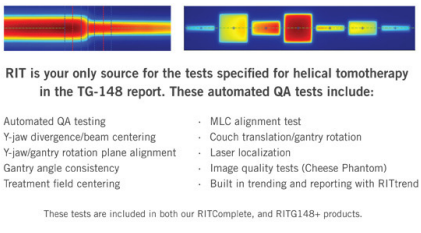

Performance of antiscatter grids in diagnostic radiology: Experimental measurements and Monte Carlo simulation studies

Heang-Ping Chan, Yoshiharu Higashida,[a] and Kunio Doi
Kurt Rossmann Laboratories for Radiologic Image Research, Department of Radiology, The University of Chicago, Chicago, Illinois 60637

(Received 30 November 1984; accepted for publication 21 March 1985)

We have devised an experimental method with which one can accurately measure the transmission of primary radiation and the transmission of total radiation by an antiscatter grid in a setting similar to a practical radiographic examination. We measured the transmission values for 27 combinations of x-ray tube potentials, phantom thicknesses, screen–film systems, and grid parameters. The standard deviation of one measurement was estimated to be 2.9% and 1.5% for the total and primary transmissions, respectively. The measured grid transmission was compared with results predicted by our Monte Carlo calculations; 92% of the measured and calculated values agree within two standard deviations. This close agreement indicates that our Monte Carlo calculation can accurately predict the performance of antiscatter grids under diagnostic imaging conditions.

I. INTRODUCTION

In radiography, a major image-degrading factor is the scattered radiation arising from the interaction of x-ray photons with the object being imaged. For example, in abdominal radiography of a 20-cm-thick patient, the scattered radiation can amount to about seven times the information-carrying primary radiation.[1] The large amount of scattered radiation has a detrimental effect on the image contrast. Various antiscatter techniques have been developed that are designed to reduce the scattered radiation incident on the image plane. The most commonly used technique at present is the use of a linear grid, which was introduced by Bucky[2] and modified by Potter.[3] A Bucky grid is employed with a reciprocating device during x-ray exposure so that the grid lines are blurred. Due to the advances in grid manufacturing technology, high strip-density grids have been introduced which can be kept stationary during x-ray exposure, since the fine grid lines appearing in a radiograph do not interfere with the perception of image detail.[4,5]

In our previous study of the performance of antiscatter grids,[4] we developed Monte Carlo simulation methods to trace photon histories in a scattering medium and in a grid. The contrast improvement factor (CIF) and the Bucky factor (BF) were employed as the benefit and cost factors, respectively, in the evaluation of grid performance. In this study, we measured the CIF and BF values for ten commonly used grids and four high strip-density grids under typical imaging conditions, and we compared the results with Monte Carlo predictions.

II. METHODS

A. Monte Carlo calculation of grid performance

We have previously described in detail the Monte Carlo methods for the simulation of photon scattering in tissue-equivalent material and in an antiscatter grid.[6–8] We have also applied these simulation methods to the evaluation of grid performance in mammography.[9] The procedure will be described briefly below.

A pencil beam of photons is incident normally on the surface of a homogeneous tissue-equivalent phantom of uniform thickness and infinite area. In the diagnostic energy range, three interaction processes—the photoelectric effect, incoherent scattering, and coherent scattering—have to be considered. In a coherent-scattering event, the scattering angle of the photon is sampled from the Thomson equation modified by the form factor for the scattering material. The form factor is calculated from the atomic form factors with the assumption that interatomic or intermolecular interference effects are negligible. For Compton scattering, the scattering angle of the photon is sampled from the Klein–Nishina equation modified by the incoherent-scattering function, which takes into account the electron binding effect. Within the phantom, a photon history is terminated when a photoelectric event occurs.

In the present study, an antiscatter grid was placed parallel to the posterior surface of the phantom. The distance from the phantom to the posterior surface of a grid was kept at 1.5 cm; thus the spacing between the phantom and a grid varied from 1.2 to 1.4 cm, depending on the thickness of the grid used. We studied linear parallel grids with infinite focal length. The interspace and the front and back covers of the grid were composed of aluminum; the radiopaque strips were made of lead. The parameters of the grids included in this study are listed in Table I.

The photons transmitted through the phantom impinged on the grid. A Monte Carlo method which can trace a photon history in an inhomogeneous phantom composed of compartments of different materials was employed for the simulation of photon diffusion in the grid.[6,8] If a coherent-scattering or incoherent-scattering event took place, the form factor or incoherent-scattering function of the material in the compartment in which the interaction occurred was used for the sampling of the deflection angle. At photon energies above the K edge of lead, if a photoelectric event took

 0094-2405/85/040449-06$01.20

TABLE I. Parameters of the 14 grids[a] included in this study.

Strip density (lines/cm)	Thickness of aluminum cover (μm)	Thickness of lead strips (μm)	Thickness of aluminum interspace (μm)	Lead-to-interspace ratio	Grid ratio	Lead content (mg/cm^2)	Grid identification
33	400	50	250	1/5	6	284	33/6/50
					8	379	33/8/50
					10	473	33/10/50
					12	568	33/12/50
					15	710	33/15/50
40	400	50	200	1/4	6	273	40/6/50
					8	364	40/8/50
					10	454	40/10/50
					12	545	40/12/50
					15	682	40/15/50
57	150	45	130	1/2.9	8	304	57/8/45
					10	380	57/10/45
					12	456	57/12/45
					16	608	57/16/45

[a] The grids were manufactured by Mitaya Manufacturing Co., Tokyo, Japan; these grids are distributed in the U. S. by Liebel–Flarsheim Co.

place in the lead strips, the computer determined whether a K_α or K_β x ray was emitted by random sampling based on the emission probability. The K x rays were assumed to be emitted isotropically from the interaction site, and their history was traced.

The recoil electron in a Compton interaction, the photoelectrons, the Auger electrons, or the fluorescence x rays other than those from the K shell were assumed to be absorbed at the interaction site. A cutoff energy of 5 keV was chosen for terminating of photon histories either inside the phantom or in the grid. At this energy, the absorption cross section of the materials considered is very large, and the photon was assumed to be absorbed locally in a photoelectric event.

The photons transmitted through the grid might be detected by a pair of fluorescent screens placed parallel to the grid. The spacing between the grid and the screens was chosen to be 1.0 cm. The energy absorbed in the screens was calculated by means of an analytical method described elsewhere.[10] The absorbed energies due to both the primary and the scattered radiation were determined by summation of all energies deposited by the primary and scattered photons, respectively, for an incident pencil beam; this is equivalent to recording the primary and scattered radiation at a point in the image plane for a plane, parallel, infinitely broad incident beam.[11]

The CIF is defined as the ratio of radiographic contrast with the grid to that without the grid. The BF is defined as the factor by which the patient exposure is increased, when an antiscatter technique is used, to maintain the film density the same as that without the grid. For grid techniques, the increase in x-ray tube loading is equal to the BF. It has been shown[6,12] that

$$\mathrm{BF} = \frac{1}{T_t} \tag{1}$$

and

$$\mathrm{CIF} = T_p \times \mathrm{BF}, \tag{2}$$

where T_t and T_p are the transmission of total and of primary radiation of the grid, respectively. The significance of using CIF and BF as the parameters for the evaluation of grid performance, as compared to other parameters such as selectivity, has been discussed extensively in our previous work.[4]

In our Monte Carlo calculations, the total and primary radiation energies absorbed in the screens under a given imaging condition without a grid were calculated from the average of ten independent runs. When a grid was employed, we determined the energies absorbed in the screens for each run by tracing the photons through the grid, and the average of ten independent runs was again taken. The values of T_t and T_p were then calculated from the ratio of the mean values of total and primary energy, respectively, absorbed in the screens with and without the grid, and the BF and CIF were derived from Eqs. (1) and (2). It should be noted that the BF and CIF of a grid depend on the imaging conditions.

We chose water as the phantom material, since the x-ray interaction properties of water are similar to those of soft tissue in the diagnostic energy range. A pair of DuPont Par Speed screens ($CaWO_4$, coating weight = 28 mg/cm^2 per screen) or a pair of Kodak Lanex Regular screens (Gd_2O_2S:Tb, coating weight = 70 mg/cm^2 per screen) was employed as the x-ray recording system. The cross section data of the phantom, the grid materials, and the screen phosphors were calculated from the elemental cross sections tabulated by Storm and Israel.[13] The atomic form factors and incoherent-scattering functions were compiled by Hubbell and Øverbø[14] and by Hubbell *et al.*,[15] respectively. The K-fluorescence yields of lead and of the heavy elements in the phosphors were tabulated by Lederer *et al.*,[16] and by Bambynek *et al.*[17]

We measured the x-ray spectra that were the input to the Monte Carlo program by using an x-ray spectrometer system with a high-resolution germanium detector.[6] The x-ray source was a Siemens tungsten-anode tube (Bi 150/30/50R) with a Siemens 3-phase 12-pulse x-ray generator (Tridoros 150G-3). The inherent filtration of the tube was 1.5-mm Al equivalent, and the added filtration was 1-mm Al for the 70- and 80-kV spectra and 2-mm Al for the 120-kV spectrum used.

B. Experimental measurement of grid performance

We used the experimental setup shown in Figs. 1 (a) and 1 (b) for measurement of the transmission of total and of primary radiation of a grid, respectively. A special device was made for moving the grid during x-ray exposure. The device includes a stationary platform on which a screen–film cassette can be placed in a fixed position, guided by rails on three sides. Above the platform there is a tray which carries the grid. A variable-speed motor drives the tray in a reciprocating motion by means of a mechanical joint that converts the circular motion of the motor to a linear oscillating motion. The device also includes a phantom stand which supports a 30×30 cm^2 water tank in a position centered at the midpoint of the grid motion. We measured the grid transmission at several settings of the motor speed and found no observable difference in the results. Therefore we used a very slow speed during the measurements, and the x-ray exposure was made when the center of the grid passed through the central ray of the x-ray beam. In this way, the loss of x-ray transmission due to grid decentering was minimized.

Our tissue-equivalent phantom was a Lucite tank with 1-cm-thick walls and an area of 30×30 cm^2, filled with water to the desired depth. A screen–film system was enclosed in a vacuum cassette, which was located on the platform at a distance of 1 cm from the grid. The vacuum cassette has a thin vinyl front surface that is essentially transparent to x-rays. A lead sheet was placed between the back screen and the aluminum backing of the cassette for reduction of backscatter.

For the measurement of total transmission, the water phantom was supported on the grid device with a phantom-to-grid spacing that varied from 1.2 to 1.4 cm, depending on the thickness of the grid. A broad-beam geometry was employed. The focal-spot-to-grid distance was 100 cm, equal to the focal length of the grids studied, and the field size was 30×30 cm^2 on the water surface. For the measurement of primary transmission, a narrow-beam geometry was used. The focal-spot-to-grid distance was increased to 145 cm, and the phantom was supported at a distance of 74 cm from its bottom to the grid. The phantom was sandwiched between two lead collimators. The anterior and the posterior collimator had circular apertures of 3.5 and 4.5 mm in diameter, respectively, defining a beam of about 14 mm in diameter on the image plane. This beam size was chosen based on a measurement of T_p made with variable collimator apertures that yielded beams from 12×12 to 58×58 mm^2 on the image plane. The results indicated that a beam area of 1.5 cm^2 provided a T_p value less than 0.004 higher than the extrapolated value for a zero beam diameter. This discrepancy was within our experimental uncertainty. For convenience, we fixed the beam size at the diameter of 14 mm for all of the T_p measurements without using the extrapolation procedure.

The x-ray source was a Siemens Bi 125/3/50RG tungsten-anode tube with a Tridoros 150G-3 generator. The tube had a total filtration of 2.5 mm Al. A large focal spot (nominal size = 1 mm) was used at 70 and 80 kV, whereas a small focal spot (nominal size = 200 μm) was used at 120 kV for reduction of the output x-ray intensity for these measurements.

We employed a high-precision focal-spot device[18] to locate the central ray of the x-ray beam. The focal spot, the grid device, and the collimators (for the measurement of primary transmission) were then carefully aligned so that the central ray impinged normally on the center of motion of the grid.

To obtain each measured transmission value, we exposed at least six films each with and without the grid, so that a range of film densities from about 0.8 to 2.2 was obtained in each case. We adjusted the radiation intensity by changing the mA setting while keeping the exposure time constant to avoid the effect of reciprocity law failure on the film densities. An MDH ionization chamber (model 10X5-6 with a model 1015 x-ray monitor) was mounted in a fixed position, as shown in Fig. 1, for measurement of the relative incident radiation for each exposure. The kV of the output x-ray beam was monitored with a Machlett Dynalyzer II so that only films exposed within $\pm$ 0.5 kV error were retained. All films were developed at the same time, together with a sensitometric calibration film of the same screen–film system ex-

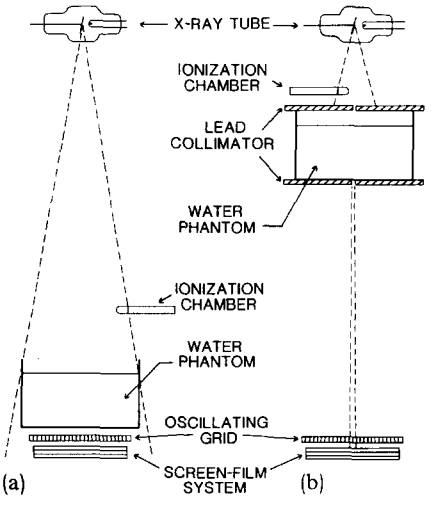

FIG. 1. Experimental setup for measurement of transmission of (a) total radiation and (b) primary radiation. The dimensions are specified in the text.

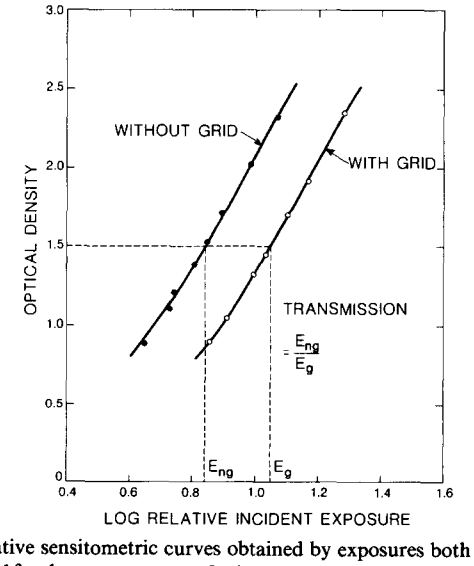

FIG. 2. Relative sensitometric curves obtained by exposures both without and with grid for the measurement of primary transmission. Imaging conditions: 80 kV, 20-cm-thick water phantom, 40 lines/cm and 8:1 ratio grid, Par/XRP system.

posed with an intensity scale x-ray sensitometer.[19] The film densities were then plotted against the log relative exposure for the cases both with and without the grid. We used the shape of the sensitometric curve to fit a smooth curve to the data points. Figure 2 shows an example of curves for a T_p measurement with a Par Speed/XRP system. The transmission of the grid was calculated as the ratio of the incident exposure without grid to that with grid for a given film density. This procedure can be applied to the measurement of both primary transmission and total transmission. In the latter case, very thin lead wires placed on top of the phantom identified the position of the central ray, so that the film densities could be measured consistently at the center of the x-ray field. Thus we avoided any uncertainty caused by field nonuniformity.

III. RESULTS

We determined grid performance for 27 combinations of x-ray tube potentials, phantom thicknesses, screen–film systems, and grid parameters. Table II shows the transmission of total radiation and the transmission of primary radiation obtained from Monte Carlo calculations and from experimental measurements. Each calculated value is the mean of ten runs; for each run, we employed 12 000–29 000 photons incident on the grid. The standard deviation of the mean varied from about 0.4% to 1.5% for the total transmission and from about 0.7% to 2.4% for the primary transmission. For the experiments, each transmission value was obtained as an average of two or three measurements. The standard deviation of one measurement was estimated to be 2.9% and 1.5% for the total and primary transmission, respectively; these percentages correspond to a standard deviation of about 0.01 in the transmission values. Figures 3 and 4 show the measured total and the measured primary transmission, respectively, plotted against the calculated values. It can be seen that the experimental values agreed with the Monte Carlo results within 0.02 except at four points. The correlation coefficients were 0.99 and 0.97 for the comparison of the total and primary transmission, respectively.

The BF and CIF derived from the measured and calculated transmission values are also listed in Table II. The performance of the grids with 40 lines/cm under various imaging conditions is compared in a CIF versus BF diagram[4] (Fig. 5) based on the relationship derived in Eq. (2). It can be seen that, for a given grid, both the CIF and BF decrease as the tube voltage increases and the phantom thickness decreases. This may be attributed in part to the increase in the transmission of scattered radiation through the grid when the photon energy increases. It may be noted from Table II, however, that T_p decreases slightly when the tube voltage increases from 70 to 80 kV. This decrease probably results from a complicated combination of changes in two quantities, namely, the spectral distribution of the transmitted primary radiation and the energy response of the screen phosphor, at different tube voltages and phantom thicknesses, with and without use of the grid.

The CIF and BF of a grid depend strongly on the energy response of the recording system, as can be seen from the

TABLE II. Measured and calculated grid performance data for various imaging conditions.

Tube potential Water thickness Screen/film	Scatter-to-primary ratio	Primary fraction	Grid identification	Monte Carlo results				Experimental results			
				T_t	T_p	BF	CIF	T_t	T_p	BF	CIF
70 kV	5.92	0.145	40/6/50	0.212	0.673	4.73	3.18	0.195	0.678	5.13	3.48
25 cm			40/8/50	0.172	0.653	5.83	3.80	0.154	0.658	6.49	4.27
Lanex Regular/OG			40/10/50	0.146	0.625	6.83	4.27	0.127	0.621	7.87	4.89
			40/12/50	0.130	0.608	7.66	4.66	0.112	0.601	8.93	5.37
80 kV	4.29	0.190	33/6/50	0.242	0.672	4.12	2.77	0.257	0.682	3.89	2.65
20 cm			33/8/50	0.201	0.644	4.97	3.20	0.210	0.649	4.76	3.09
Lanex Regular/OG			33/10/50	0.173	0.617	5.77	3.56	0.181	0.595	5.52	3.29
			33/12/50	0.154	0.585	6.48	3.79	0.159	0.581	6.29	3.65
			33/15/50	0.135	0.553	7.39	4.08	0.140	0.544	7.14	3.89
			40/6/50	0.246	0.665	4.07	2.71	0.262	0.677	3.82	2.58
			40/8/50	0.203	0.637	4.92	3.13	0.213	0.632	4.69	2.97
			40/10/50	0.177	0.622	5.64	3.50	0.170	0.620	5.88	3.65
			40/12/50	0.157	0.597	6.36	3.79	0.158	0.602	6.33	3.81
			40/15/50	0.140	0.565	7.15	4.04	0.131	0.566	7.63	4.32
			57/8/45	0.224	0.659	4.46	2.94	0.242	0.675	4.13	2.79
			57/10/45	0.195	0.644	5.13	3.31	0.199	0.653	5.03	3.28
			57/12/45	0.175	0.628	5.71	3.58	0.168	0.588	5.95	3.50
			57/16/45	0.148	0.594	6.74	4.00	0.133	0.563	7.52	4.23
80 kV	6.77	0.129	40/6/50	0.177	0.646	5.65	3.65	0.192	0.658	5.21	3.43
20 cm			40/8/50	0.143	0.617	6.98	4.31	0.151	0.633	6.62	4.19
Par Speed/XRP			40/10/50	0.123	0.597	8.15	4.87	0.127	0.591	7.87	4.65
			40/12/50	0.108	0.571	9.28	5.30	0.110	0.565	9.09	5.14
			40/15/50	0.095	0.538	10.55	5.67	0.092	0.527	10.87	5.73
120 kV	3.19	0.239	40/6/50	0.327	0.704	3.06	2.16	0.355	0.728	2.82	2.05
15 cm			40/8/50	0.276	0.683	3.62	2.47	0.301	0.699	3.32	2.32
Lanex Regular/OG			40/10/50	0.242	0.663	4.13	2.74	0.264	0.682	3.79	2.58
			40/12/50	0.219	0.641	4.57	2.93	0.241	0.663	4.15	2.75

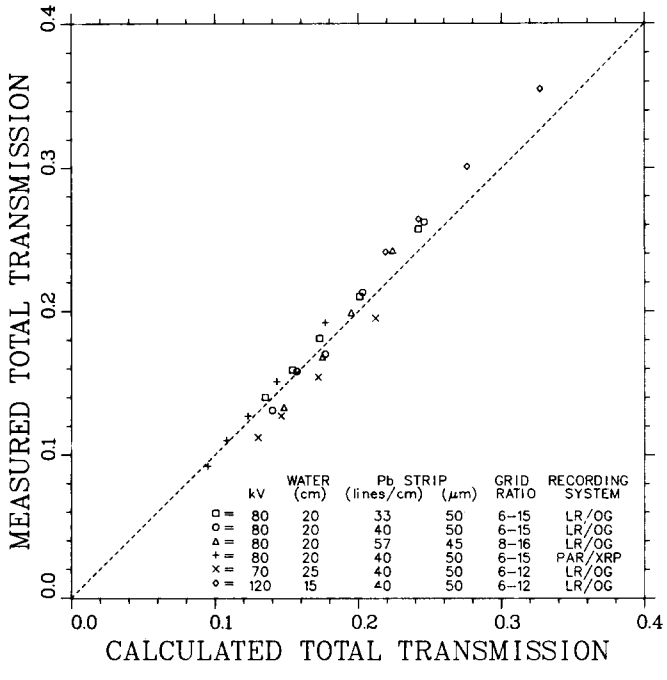

FIG. 3. Comparison of measured total transmission with total transmission predicted by Monte Carlo calculations for various imaging conditions and grids. The dashed line indicates the expected curve if perfect agreement is obtained.

curve for the Lanex Regular screens and that for the Par Speed screens (Fig. 5). The large reduction in the recorded T_t leads to an increase in the BF and CIF for the Par Speed system. However, the ratio CIF/CIF$_{max}$ (where CIF$_{max}$ is the maximum CIF achievable by an ideal antiscatter technique with a given recording system and is equal to the reciprocal of the recorded primary fraction) for a given grid is higher for the Lanex Regular system than for the Par Speed system. This implies that the relative contrast improvement efficiency of a grid actually decreases when the Par Speed screens are used as the recording system.[1]

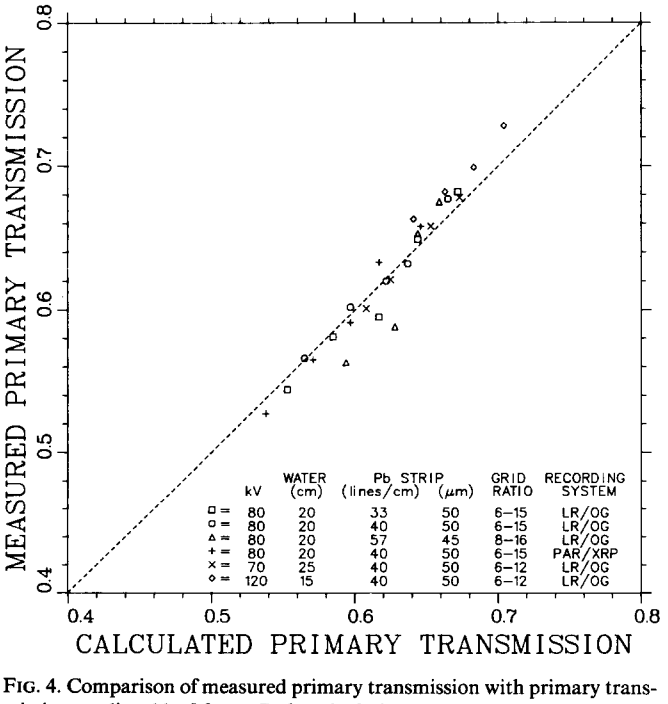

FIG. 4. Comparison of measured primary transmission with primary transmission predicted by Monte Carlo calculations.

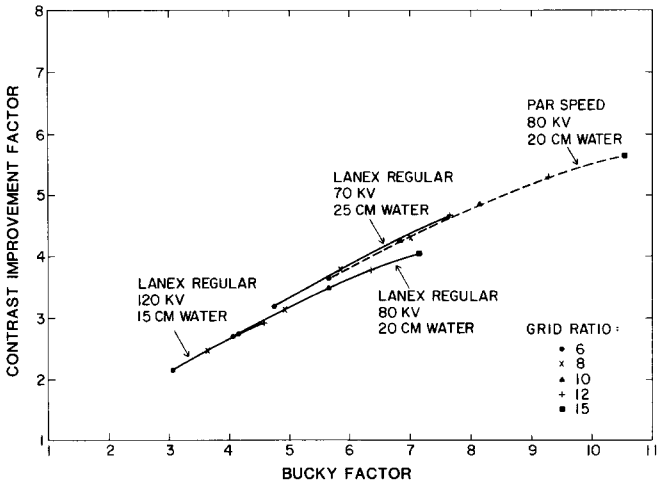

FIG. 5. CIF vs BF diagram for the comparison of grid performance under various imaging conditions. Strip density of grids: 40 lines/cm; lead-to-interspace ratio: 1/4; thickness of lead strips: 50 μm.

IV. DISCUSSION AND CONCLUSION

In this study, we have devised an experimental method with which we can accurately measure the transmission of primary radiation and the transmission of total radiation by an antiscatter grid in a setting similar to a practical imaging situation. The main differences between our method and that recommended by the International Commission on Radiation Units and Measurements (ICRU)[20] lie in the x-ray detectors used and the way in which the radiation transmission values are derived. Although the ICRU method is useful in providing a standard from which the relative effectiveness of various grids measured by different investigators or manufacturers can be compared, it cannot be used for quantifying of the grid performance parameters for a specific imaging condition. As can be seen from the data in Table II, the transmission values for the same grid vary over a wide range that depends on the phantom, the tube voltage, as well as the energy response of the recording system. It is therefore important, when a radiographic examination is performed with the use of an antiscatter grid, to determine the dose increase factor and the contrast improvement factor based on the grid performance measured under similar conditions.

The measured radiation transmission of the grids agrees closely with that obtained by Monte Carlo calculations, as discussed in the preceding section; nevertheless, small systematic deviations can be observed between the measured and the calculated values for grids of the same strip density and under the same imaging conditions. For example, at 70 kV the measured T_t values are consistently slightly lower than the calculated values, whereas this trend is reversed at 120 kV. At 80 kV, the measured T_p values are higher than the calculated values for low-ratio grids and are lower for high-ratio grids at strip densities of 33 and 57 lines/cm. Similar trends can be identified for some other conditions shown in Table II. These systematic discrepancies may be caused by differences between the spectral distributions of the incident x-rays used in the calculations and those used in the experiments, since the x-ray tube mounted in our x-ray spectrometer was different from that used for the transmission mea-

surements. The possible difference between the parameters in a practical grid and the nominal values employed as input data in our Monte Carlo calculations may also contribute to the discrepancies.

We have chosen the CIF and the BF as the parameters for the evaluation of grid performance because they represent the benefit (gain in contrast) and the cost (increase in patient dose), respectively, of using a grid. These two factors depend on T_p and T_t, which can be measured directly by experiments. When these performance parameters are plotted on a CIF versus BF diagram, the tradeoff between the benefit and the cost of using grids with various design parameters or using grids under various imaging conditions can be compared directly and unambiguously.[4] On the other hand, the parameters such as selectivity and T_p, which are commonly used as indicators of grid performance,[21] are not directly related to the benefit and cost of using a grid. In fact, since CIF levels off at large selectivity values for a given scatter-to-primary ratio,[6,21] the use of a grid which has a much larger selectivity than another grid may not result in a much larger gain in contrast, whereas the patient exposure may become unacceptably high. Furthermore, two different grids which have equal selectivities may have very different BFs, because a reduction in T_p and T_s (transmission of scattered radiation) by the same factor leads to the same selectivity value while the T_t of one grid will become much smaller than that of the other. This occurs when the grid design parameters are not chosen properly.[4] Therefore the use of selectivity as an indicator of the effectiveness of a grid can be misleading, and we believe that selectivity values should not be used for the comparison of grid performance.

Our results confirm that the variation in the CIF and BF values for a given grid among different imaging conditions can be larger than the variation of these factors among different grids. Therefore a meaningful comparison of grid performance can be accomplished only if the grids are evaluated under similar conditions. However, a more thorough investigation should be conducted on the dependence of the relative performance of grids on imaging conditions. The information obtained will be useful for the optimization of grid design under various imaging conditions.

The results of this investigation indicate that the Monte Carlo calculations can accurately predict the performance of antiscatter grids under diagnostic imaging conditions. The computer simulation method facilitates the comparison of the effectiveness of grids with various design parameters, by taking into consideration the incident x-ray spectrum, phantom material and size, and the energy response of the recording system. Thus the grid design for a given radiographic procedure can be optimized without the construction of many experimental grids and without tedious measurements. We have applied our Monte Carlo programs to the study of the effects of various grid parameters (strip density, grid ratio, lead-to-interspace ratio, interspace material, and lead content) on the contrast improvement capability and the dose requirement.[4] The grid performance was evaluated by means of a CIF versus BF diagram. The results of these studies have led to the development of high-strip-density grid techniques for both general radiographic[5] and mammographic examinations.[9]

ACKNOWLEDGMENTS

This work was supported in part by USPHS Grant No. CA 24806. We are grateful to Mr. N. Iida, Mitaya Manufacturing Co., for his support of this work and for providing technical information on the grids, to M. Carlin for technical assistance, to E. Lanzl for editing the manuscript, and to E. Ruzich for secretarial assistance.

[a] Present address: College of Medical Science, Kumamoto University, 24-1 Kuhonji, Kumamoto, Japan.

[1] H. -P. Chan and K. Doi, RadioGraphics **2**, 378 (1982)
[2] G. Bucky, U. S. Patent No. 1,164,987 (1915).
[3] H. E. Potter, Am. J. Roentgenol. **7**, 292 (1920).
[4] H. -P. Chan and K. Doi, Phys. Med. Biol. **27**, 785 (1982).
[5] K. Doi, P. H. Frank, H. -P. Chan, C. J. Vyborny, S. Makino, N. Iida, and M. Carlin, Radiology **147**, 575 (1983).
[6] H. -P. Chan, Ph. D. dissertation (The University of Chicago, 1981).
[7] H. -P. Chan and K. Doi, Phys. Med. Biol. **28**, 109 (1983).
[8] H. -P. Chan and K. Doi, in *Monte Carlo Simulation in the Radiological Sciences*, edited by R. L. Morin (CRC, Florida, in press).
[9] H. -P. Chan, P. H. Frank, K. Doi, N. Iida, and Y. Higashida, Radiology **154**, 807 (1985).
[10] H. -P. Chan and K. Doi, Phys. Med. Biol. **28**, 565 (1983).
[11] H. -P. Chan and K. Doi, Med. Phys. **12**, 152 (1985).
[12] W. Hondius Boldingh, Acta Radiol. **55**, 225 (1961).
[13] E. Storm and H. I. Israel, Nucl. Data Tables **A 7**, 565 (1970).
[14] J. H. Hubbell and I. Øverbø, J. Phys. Chem. Ref. Data **8**, 69 (1979).
[15] J. H. Hubbell, W. J. Veigele, E. A. Briggs, R. T. Brown, D. T. Cromer, and R. J. Howerton, J. Phys. Chem. Ref. Data **4**, 471 (1975).
[16] C. M. Lederer, J. M. Hollander, and I. Perlman, *Table of Isotopes*, 6th ed. (Wiley, New York, 1968), p. 571.
[17] W. Bambynek, B. Crasemann, R. W. Fink, H. -U. Freund, H. Mark, C. D. Swift, R. E. Rice, and P. V. Rao, Rev. Mod. Phys. **44**, 716 (1972).
[18] K. Doi, B. Fromes, and K. Rossmann, Med. Phys. **2**, 268 (1975).
[19] A. G. Haus and K. Rossmann, Radiology **94**, 673 (1970).
[20] International Commission on Radiation Units and Measurements Report No. 10f, 1963.
[21] K. -G. Strid, Acta Radiol. Suppl. **351** (1976).